

Orbital Kondo effect in double quantum dots

Piotr Trocha^{1,*}

¹*Department of Physics, Adam Mickiewicz University, 61-614 Poznań, Poland*

(Dated: October 16, 2018)

Orbital Kondo effect in a system of two single-level quantum dots attached to external electron reservoirs is considered theoretically. The dots are coupled *via* direct hopping term and Coulomb interaction. The Kondo temperature is evaluated from the scaling approach and slave boson technique. The later method is also used to calculate linear conductance of the system. Nonlinear conductance, in turn, is calculated in terms of the nonequilibrium Green function formalism.

PACS numbers: 72.15.Qm, 73.23.-b, 73.63.Kv

I. INTRODUCTION

Kondo effect in electronic transport through quantum dots (QDs) strongly coupled to external leads is a many body phenomenon which has been extensively studied in the last two decades^{1–11}. Spin fluctuations in the dot, generated by coupling of the dot to external leads, give rise to a narrow peak in the dot's density of states (DOS) at the Fermi level. This Rado-Suhl resonance results in enhanced transmission through the dot, and leads to the unitary limit of the linear conductance G at zero temperature, $G = 2e^2/h$. The enhanced transmission is suppressed when a bias voltage is applied, and this leads to the so-called zero-bias (Kondo) anomaly in differential conductance. The above described phenomenon arises from the two-fold spin degeneracy, and is often referred to as the spin Kondo effect. However, the Kondo phenomenon may also appear when the spin degree of freedom is replaced by any two-valued quantum number, e.g. the one associated with an orbital degree of freedom (the orbital Kondo effect)¹². A minimal realization of the orbital (spinless) Kondo phenomenon requires two orbital discrete levels coupled to external leads^{13,14}. This can be realized for instance in two single-level quantum dots coupled to external electrodes^{15–24}. Coherent superposition of virtual tunneling events, in which one electron tunnels from the dot QD1 (QD2) to one of the leads and then simultaneously another electron tunnels to the dot QD2 (QD1), leads to the Kondo resonance at low temperatures.

In this paper we consider theoretically the Kondo phenomenon in electronic transport through two QDs coupled, in general, *via* both Coulomb interaction and hopping term. To evaluate the level renormalization and Kondo temperature of the system we use the scaling approach. The Kondo temperature is also evaluated from the slave boson technique. Additionally, the latter technique is used to calculate the linear conductance. Then, the nonequilibrium Green function formalism is used to calculate the local density of states (LDOS) for both dots and transport characteristics (differential conductance) in the nonlinear response regimes. To calculate the relevant Green's functions from the corresponding equations of motion we apply the decoupling scheme introduced in

Ref. [4].

The orbital Kondo effect in double quantum dot (DQD) systems was analyzed e.g. in Ref. [18]. However, our results are different, and the key difference consists in a different symmetry of the couplings to external leads. Moreover, we use various techniques including scaling, slave boson, and nonequilibrium Green function formalisms. Apart from this, we apply a different method to evaluate the lesser Green function. The paper is organized as follows. In section 2 we describe the model of a double quantum dot system. Renormalization of the dots' levels and the Kondo temperature are discussed in section 3 in terms of the scaling approach. The slave boson technique is briefly described in section 4 and is used there to estimate the Kondo temperature and calculate the linear conductance. Basic formula for nonequilibrium Green functions and the corresponding numerical results on the conductance and LDOS are presented and discussed in section 5. Summary and final conclusions are given in section 6.

II. MODEL

We consider two coupled single-level quantum dots connected to nonmagnetic electron reservoirs as shown schematically in Fig.1. Each dot is attached to separate source and drain leads, so the tunneling paths *via* the two orbitals can be analyzed separately as in recent experiments^{15,16}. We consider the case when each dot is coupled symmetrically to the leads, while the corresponding coupling strengths for both dots may be different. Moreover, our considerations are limited to the case of spinless electrons, which can be realized experimentally for instance by applying a sufficiently strong external magnetic field lifting the spin degeneracy.

The system under consideration can be described by the extended Anderson Hamiltonian of the general form

$$\hat{H} = \hat{H}_{\text{leads}} + \hat{H}_{\text{DQD}} + \hat{H}_{\text{tunnel}}. \quad (1)$$

The first term, \hat{H}_{leads} , describes here the four leads in the non-interacting quasi-particle approximation, $\hat{H}_{\text{leads}} = \hat{H}_{L1} + \hat{H}_{L2} + \hat{H}_{R1} + \hat{H}_{R2}$, with $\hat{H}_{\beta i}$ being the Hamiltonian of the left ($\beta = L$) and right ($\beta = R$) lead attached to the

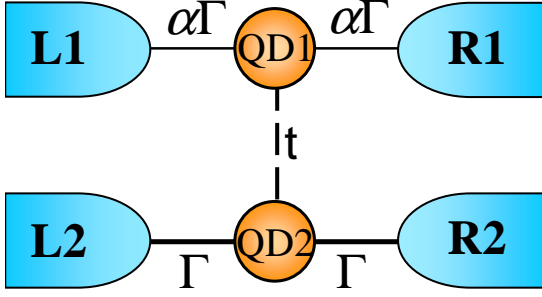


FIG. 1: (color online) Schematic picture of the double quantum dot system coupled to external leads.

i th dot ($i = 1, 2$), $\hat{H}_{\beta i} = \sum_{\mathbf{k}} \epsilon_{\mathbf{k}\beta i} c_{\mathbf{k}\beta i}^\dagger c_{\mathbf{k}\beta i}$ (for $\beta = L, R$ and $i = 1, 2$). Here, $c_{\mathbf{k}\beta i}^\dagger$ ($c_{\mathbf{k}\beta i}$) is the creation (annihilation) operator of an electron with the wave vector \mathbf{k} in the lead βi , whereas $\epsilon_{\mathbf{k}\beta i}$ denotes the corresponding single-particle energy.

The second term of the Hamiltonian (1) describes the double quantum dot system,

$$\hat{H}_{DQD} = \sum_i \epsilon_i d_i^\dagger d_i + t(d_1^\dagger d_2 + h.c.) + U n_1 n_2, \quad (2)$$

where $n_i = d_i^\dagger d_i$ is the particle number operator ($i = 1, 2$), ϵ_i is the discrete energy level of the i -th dot, t denotes the inter-dot hopping parameter (assumed real), and U is the inter-dot Coulomb integral.

The last term, H_T , of Hamiltonian (1) describes electron tunneling between the leads and dots, and takes the form

$$\hat{H}_T = \sum_{\mathbf{k}} \sum_{\beta i} (V_{i\mathbf{k}}^\beta c_{\mathbf{k}\beta i}^\dagger d_i + h.c.), \quad (3)$$

where $V_{i\mathbf{k}}^\beta$ are the relevant tunneling matrix elements. Coupling of the dots to external leads can be parameterized in terms of $\Gamma_i^\beta(\epsilon) = 2\pi \sum_{\mathbf{k}} V_{i\mathbf{k}}^\beta V_{i\mathbf{k}}^{\beta*} \delta(\epsilon - \epsilon_{\mathbf{k}\beta i})$. We assume that Γ_i^β is constant within the electron band, $\Gamma_i^\beta(\epsilon) = \Gamma_i^\beta = \text{const}$ for $\epsilon \in \langle -D, D \rangle$, and $\Gamma_i^\beta(\epsilon) = 0$ otherwise. Here, $2D$ denotes the electron band width. We assume the dots are symmetrically coupled to the leads, $\Gamma_1^L = \Gamma_1^R = \alpha\Gamma$, and $\Gamma_2^L = \Gamma_2^R = \Gamma$. The parameter α takes into account difference in the coupling of the two dots to external leads. Note, that for these parameters, each dot separately is coupled symmetrically to the two leads.

III. LEVEL RENORMALIZATION AND KONDO TEMPERATURE

Coupling of the dots to external leads gives rise to renormalization of the energy levels of both dots. In this section we use the scaling approach to derive some general formula for the renormalized levels in unbiased

system. From the scaling equations we also estimate the relevant Kondo temperature. The derived results will be used subsequently for interpretation of the numerical results on electronic transport and LDOS.

A. Renormalization of the QDs' levels

Now, we apply the scaling technique to derive renormalized dots' energy levels and begin with the limit of $t = 0$. In the scaling approach, the high-energy excited states (in the energy region of width δD at the band edges) are removed, but their impact on the system is taken into account *via* renormalized parameters of the Hamiltonian. Here, we consider only second order processes, where the leads' electrons are scattered to the band edges and back. To perform scaling we assume $\epsilon_i + U \gg D \gg |\epsilon_i|$. After integrating out the band edge states we arrive at the following renormalized parameters;

$$\tilde{\epsilon}_i = \epsilon_i - E_0 + \frac{\Gamma_i}{2\pi} \frac{\delta D}{D}, \quad (4)$$

where E_0 is the energy of empty DQD system (initially $E_0 = 0$) and the index $\tilde{i} = 1$ for $i = 2$ and $\tilde{i} = 2$ for $i = 1$. Here, Γ_i is defined as $\Gamma_i = \Gamma_i^L + \Gamma_i^R$. This procedure leads to the following scaling equation:

$$\frac{d\tilde{\epsilon}_i}{d \ln D} = -\frac{\Gamma_{\tilde{i}}}{2\pi}, \quad (5)$$

and to the level separation,

$$\Delta\tilde{\epsilon} = \tilde{\epsilon}_1 - \tilde{\epsilon}_2 = \epsilon_1 - \epsilon_2 + \frac{(\Gamma_2 - \Gamma_1)}{2\pi} \ln \left(\frac{D}{\tilde{D}} \right), \quad (6)$$

where \tilde{D} is the band width at the end of scaling procedure. When $\epsilon_1 = \epsilon_2 = \epsilon_0$, the above equation shows that the initial degeneracy is generally lifted.

Scaling in the presence of direct tunneling between the dots, $t \neq 0$, is more complex in a general case. However, we restrict our considerations to some limiting cases, i.e. when the hoping term is weak, $|t|/\Gamma \ll 1$, and when $|t|/\Gamma \gg 1$. If the bare dots' levels are degenerate, the direct hopping term generally lifts the degeneracy. The two eigenstates of the coupled quantum dots isolated from the leads correspond to the antibonding and bonding states, with the eigenenergies $\epsilon_{\pm} = (\epsilon_1 + \epsilon_2)/2 \pm \sqrt{\Delta\epsilon^2 + t^2}$, where $\Delta\epsilon = (\epsilon_1 - \epsilon_2)/2$. When the hoping term is small, one can first perform scaling of the bare dots' levels and then incorporate nonzero t by substituting $\epsilon_{1(2)}$ by $\tilde{\epsilon}_{1(2)}$ in the above expression for ϵ_{\pm} . The situation changes when tunneling coupling between the dots is larger than the dot-lead coupling. To find the relevant energy levels involved in the Kondo effect, one has to diagonalize the dot's Hamiltonian first (transformation to the bonding and antibonding states), and then perform scaling for the energy levels ϵ_+ and ϵ_- . The corresponding scaling

equation has the form

$$\frac{d\tilde{\epsilon}_{\pm}}{d\ln D} = -\frac{\Gamma_{\mp}}{2\pi}, \quad (7)$$

which is similar to Eq.(5). However, the effective coupling of the new states to the leads acquires now the form $\Gamma_{\pm} = \Gamma_1 + \Gamma_2$. Thus, the level separation in the limit of strong hopping term is independent of the couplings Γ_{\pm} as they are both the same, $\Gamma_+ = \Gamma_-$.

B. Kondo temperature

Now we evaluate the Kondo temperature for $t = 0$ and $\epsilon_1 = \epsilon_2 = \epsilon_0$ using the 'poor man' scaling approach²⁶. To pursue this method one has to derive first the Kondo Hamiltonian by performing the Schrieffer-Wolf transformation. Then, the band width is reduced by eliminating states with energy $D - \delta D \leq |\epsilon_{\mathbf{k}\beta i}| \leq D$ and introducing a new effective Kondo Hamiltonian, which has the same form as the initial one, but with renormalized parameters \tilde{J}_+ , \tilde{J}_- , \tilde{J}_{z1} and \tilde{J}_{z2} . All information on the high energy excitations is incorporated into these renormalized parameters.

To apply the renormalization group procedure we first reformulate the definitions of the coupling parameters Γ_i in the following way: $\Gamma_1 = 2\alpha\Gamma \equiv \tilde{\Gamma}(1 - \tilde{p})$ and $\Gamma_2 = 2\Gamma \equiv \tilde{\Gamma}(1 + \tilde{p})$, so that $\tilde{\Gamma} = (\alpha + 1)\Gamma$ and $\tilde{p} = (1 - \alpha)/(1 + \alpha)$. After performing scaling procedure one arrives at the following scaling equations;

$$\frac{d(\rho\tilde{J}_{\pm})}{d\ln D} = -\rho\tilde{J}_{\pm}(\rho\tilde{J}_{z1} + \rho\tilde{J}_{z2}), \quad (8)$$

$$\frac{d(\rho\tilde{J}_{zi})}{d\ln D} = -2(\rho\tilde{J}_{\pm})^2, \quad (9)$$

where $\rho = \rho_1 = \rho_2$, with $\rho_i = \sum_{\beta} \rho_{\beta i}$, and $\rho_{\beta i}$ being the density of states in the lead βi ($\beta = L, R$ and $i = 1, 2$). To solve these equations we first find the scaling trajectories $(\rho\tilde{J}_{\pm})^2 - (\rho\tilde{J}_{z1})(\rho\tilde{J}_{z2}) = 0$ and $\rho\tilde{J}_{z1} - \rho\tilde{J}_{z2} = \text{const} \equiv \rho J_{z1}^0 - \rho J_{z2}^0 = \tilde{p}\rho(J_{z1}^0 + J_{z2}^0)$. This allows us to write only one scaling equation instead of the two coupled equations (8) and (9),

$$\frac{d(\rho\tilde{J}_{zi})}{d\ln D} = -2(\rho\tilde{J}_{zi})[\rho\tilde{J}_{zi} \mp \rho\tilde{p}(J_{z1}^0 + J_{z2}^0)], \quad (10)$$

for $i = 1, 2$. One actually continues the scaling process until $D \approx k_B T_K$. Solving Eq. (10) one finds the Kondo temperature as the relevant scaling invariant,

$$T_K = \tilde{D} \exp \left\{ -\frac{1}{\rho(J_{z1}^0 + J_{z2}^0)} \frac{\text{arctanh}(\tilde{p})}{\tilde{p}} \right\}, \quad (11)$$

with $\rho(J_{z1}^0 + J_{z2}^0) = \frac{2\tilde{\Gamma}}{\pi} \frac{U}{|\epsilon_0|(\epsilon_0 + U)}$. The above formula resembles the corresponding one for the Kondo temperature in a single QD coupled to ferromagnetic leads²⁷,

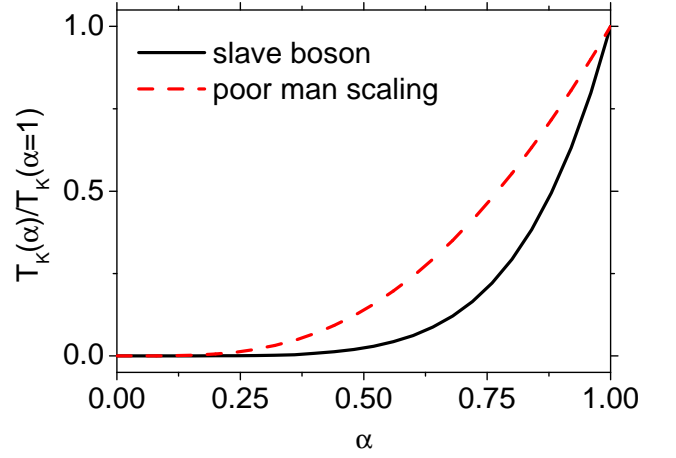


FIG. 2: Normalized Kondo temperature as a function of the parameter α , obtained from the scaling method for $U = 50\Gamma$ and from the slave boson technique for $U = \infty$. The other parameters are $\epsilon_0 = -3.5\Gamma$ and $t = 0$.

where instead of \tilde{p} we have spin polarization p of the leads.

Variation of the Kondo temperature with the parameter α is shown in Fig.2 (dashed line). T_K reaches maximum value for $\alpha = 1$ ($\tilde{p} = 0$) and vanishes for $\alpha \rightarrow 0$ ($\tilde{p} = 1$). This behavior is similar to that for spin Kondo phenomenon in a QD coupled to ferromagnetic leads. We also note that our results are in agreement with those obtained in Ref.[28], where the authors mapped spinless DQD system onto a spinful generalized Anderson model.

IV. SLAVE BOSON APPROACH

To estimate the Kondo temperature and calculate conductance in the linear response regime, we apply now the slave boson technique for $U \rightarrow \infty$ ²⁹. This method relies on introducing auxiliary operators for the dots, and replacing the electron creation and annihilation operators by $f_i^\dagger b$ and $b^\dagger f_i$, respectively. Here, b^\dagger creates an empty state, whereas f_i^\dagger creates a singly occupied state with an electron in the i -th dot. To eliminate non-physical states, the following constraint has to be imposed on the new quasi-particles,

$$Q = \sum_i f_i^\dagger f_i + b^\dagger b = 1. \quad (12)$$

The above constraint prevents double occupancy of the system (the DQD system is either empty or singly occupied).

In the mean field approximation (MFA), the boson field b is replaced by an independent of time real number, $b(t) \rightarrow \langle b(t) \rangle \equiv \bar{b}$. This approximation, however, restricts considerations to the low bias regime ($eV \ll |\epsilon_i|$).

Introducing now the following renormalized parameters: $\bar{t} = t\bar{b}^2$, $\bar{V}_{i\mathbf{k}}^\beta = V_{i\mathbf{k}}^\beta \bar{b}$, and $\bar{\epsilon}_i = \epsilon_i + \lambda$, where λ is the corresponding Lagrange multiplier, one can write the effective MF Hamiltonian as

$$\begin{aligned} \hat{H}^{MF} = & \sum_{\mathbf{k}} \sum_{\beta i} \varepsilon_{\mathbf{k}\beta i} c_{\mathbf{k}\beta i}^\dagger c_{\mathbf{k}\beta i} + \sum_i \bar{\epsilon}_i f_i^\dagger f_i + (\bar{t} f_1^\dagger f_2 + \text{h.c.}) \\ & + \sum_{\mathbf{k}} \sum_{\beta i} (\bar{V}_{i\mathbf{k}}^\beta c_{\mathbf{k}\beta i}^\dagger f_i + \text{h.c.}) + \lambda (\bar{b}^2 - 1). \end{aligned} \quad (13)$$

The unknown parameters, \bar{b} and λ , have to be found self-consistently from the following equations;

$$\bar{b}^2 - i \sum_i \int \frac{d\varepsilon}{2\pi} \langle \langle f_i | f_i^\dagger \rangle \rangle_\varepsilon^< = 1, \quad (14)$$

$$-i \sum_i \int \frac{d\varepsilon}{2\pi} (\varepsilon - \bar{\epsilon}_i) \langle \langle f_i | f_i^\dagger \rangle \rangle_\varepsilon^< + \lambda \bar{b}^2 = 0, \quad (15)$$

where $\langle \langle f_i | f_i^\dagger \rangle \rangle_\varepsilon^<$ is the Fourier transform of the lesser Green function defined as $G_{ii}^<(t, t') \equiv \langle \langle f_i(t) | f_i^\dagger(t') \rangle \rangle^< = i \langle f_i^\dagger(t') f_i(t) \rangle$. These equations follow from the constraint imposed on the slave boson field, Eq. (12), and from the equation of motion for the slave boson operator. The lesser Green functions $\langle \langle f_i | f_i^\dagger \rangle \rangle_\varepsilon^<$ as well as the retarded Green functions $\langle \langle f_i | f_i^\dagger \rangle \rangle_\varepsilon^r$ (the latter ones are required in the further calculations, too) have been determined from the corresponding equations of motion.

The Kondo temperature can be introduced as¹¹

$$T_K \equiv \sqrt{\bar{\epsilon}_0^2 + \bar{\Gamma}^2}, \quad (16)$$

with $\bar{\Gamma} = \bar{b}^2(\Gamma_1 + \Gamma_2)$ and $\bar{\epsilon}_1 = \bar{\epsilon}_2 = \bar{\epsilon}_0$. Variation of the Kondo temperature (evaluated from the above equation) with the parameter α is shown in Fig.2 (solid line).

To study charge transport we assume the same electrochemical potentials for the left leads and also equal electrochemical potentials of the right leads. The linear conductance is then calculated from the Landauer formula, in which the transmission matrix is taken at the Fermi level. More specifically linear conductance is given by the formula

$$G_{V \rightarrow 0} = \lim_{V \rightarrow 0} \frac{dJ}{dV}, \quad (17)$$

where J is current calculated at temperature $T = 0K$ ³². The slave boson technique in the form presented above, however, does not take into account the level renormalization described in the preceding sections. Therefore, to include this renormalization we replace the bare dot levels by the renormalized ones (keeping the notation used for the bare dot levels). Alternatively one may say that the renormalization is tuned out by external gate voltages. In Fig.3 the linear conductance is shown as a function of the dots' energy level, $\epsilon_1 = \epsilon_2 = \epsilon_0$, and for

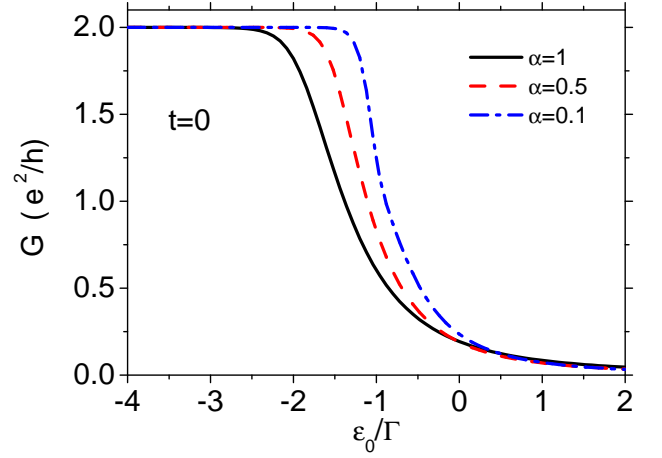


FIG. 3: Linear conductance vs. dots' level position, $\epsilon_1 = \epsilon_2 = \epsilon_0$, for indicated values of α and $t = 0$, obtained from the slave boson method for $U \rightarrow \infty$. The level splitting due to renormalization is tuned out by external gates.

indicated values of the parameter α . The linear conductance reaches the unitary limit for $\epsilon_0 \ll -\Gamma$. This limit is achieved owing to the tuning out the level splitting due to renormalization. From this figure also follows, that the Kondo temperature decreases with decreasing α , in agreement with the above discussion and Fig.2.

V. NON-EQUILIBRIUM GREEN FUNCTION APPROACH

Electric current flowing through a biased system is determined by nonequilibrium retarded, advanced, and lesser Green functions of the dots, and can be calculated from the formula derived by Meir et al²⁵. In turn, to calculate the retarded (advanced) Green functions $G_{ij}^{r(a)}(\epsilon)$, we have applied the equation of motion method (EOM). Within this method one writes first the equation of motion for the causal Green function $G_{ij}(\epsilon)$, which generates new Green functions. Then, one writes the equations of motion for these new Green functions, which in turn contain new higher-order Green functions. The latter ones have to be calculated approximately. To close the set of equations for the Green functions we have applied the decoupling scheme introduced in Ref.[4]. Although such an approximation does not describe properly the zero temperature limit, it is sufficient to describe the Kondo phenomenon close to the Kondo temperature. Detailed expressions for these Green functions are shown in the Appendix.

The retarded/advanced Green functions contain occupation numbers, n_i , and the interdot correlators, $n_{i\bar{i}} = \langle a_i^\dagger d_{\bar{i}} \rangle$, which can be calculated from the identities

$$n_i = -i \int \frac{d\epsilon}{2\pi} G_{ii}^<(\epsilon), \quad (18)$$

$$n_{i\bar{i}} = -i \int \frac{d\epsilon}{2\pi} G_{i\bar{i}}^<(\epsilon). \quad (19)$$

Thus, we still need the lesser Green functions $G_{ij}^<(\epsilon)$. However, one can note that instead of $G_{ij}^<(\epsilon)$, only $\int d\epsilon G_{ij}^<(\epsilon)$ is needed. This quantity can be found exactly (in contrast to the approach based on the Ng's approximation³⁰) and to do this we apply the Heisenberg equation of motion for the operators $d_j^\dagger(t)d_i(t)$. Then, one takes average from the obtained equation and makes use of the fact that $\langle (d/dt)d_j^\dagger(t)d_i(t) \rangle = 0$ in a steady state. As a result one obtains the following equations;

$$\begin{aligned} & t(n_{i\bar{i}} - n_{\bar{i}i}) - i\Gamma_i n_i \\ &= \sum_{\beta} \int \frac{d\epsilon}{2\pi} f_{\beta}(\epsilon) \Gamma_i^{\beta} (G_{ii}^r - G_{ii}^a), \end{aligned} \quad (20)$$

$$\begin{aligned} & t(n_i - n_{\bar{i}}) + (\epsilon_{\bar{i}} - \epsilon_i) n_{i\bar{i}} - \frac{i}{2} (\Gamma_i n_{i\bar{i}} + \Gamma_{\bar{i}} n_{\bar{i}i}) \\ &= \sum_{\beta} \int \frac{d\epsilon}{2\pi} f_{\beta}(\epsilon) [\Gamma_i^{\beta} G_{ii}^r - \Gamma_{\bar{i}}^{\beta} G_{\bar{i}\bar{i}}^a]. \end{aligned} \quad (21)$$

These equations, together with the appropriate equations for the retarded/advanced Green functions, have to be solved numerically in a self-consistent way.

The basic transport characteristics of the system, like conductance and differential conductance can be calculated numerically using the formulas derived above. The local density of states (LDOS) for the i -th dot can be calculated as

$$D_i = -\frac{1}{\pi} \Im [G_{ii}^r(\epsilon)], \quad (22)$$

where $\Im[A]$ denotes the imaginary part of A .

The approximation scheme used to calculate the nonequilibrium Green functions does not take into account the level renormalization described in the preceding sections. Therefore, to take this renormalization into account we replace the bare dot levels by the renormalized ones (keeping the notation used for the bare dot levels), similarly as in the case of slave boson technique. However, one should bear in mind that the presented EOM approach just renormalizes the bare dot's energy levels due to real part of the corresponding self-energies. This renormalization can be seen looking at the position of the broad maximum in LDOS (see Fig.4). However, the used decoupling scheme does not take it properly and thus does not lead to the expected splitting of the zero bias anomaly. In the following numerical calculations we assume equal dot energy levels, $\epsilon_i = \epsilon_0$ (for $i = 1, 2$) (ϵ_0 is measured from the Fermi level of the leads in equilibrium, $\mu_{Li} = \mu_{Ri} = 0$). Apart from this, we assume $\epsilon_0 = -3.5\Gamma$, the bandwidth $2D = 500\Gamma$, and $U = 50\Gamma$.

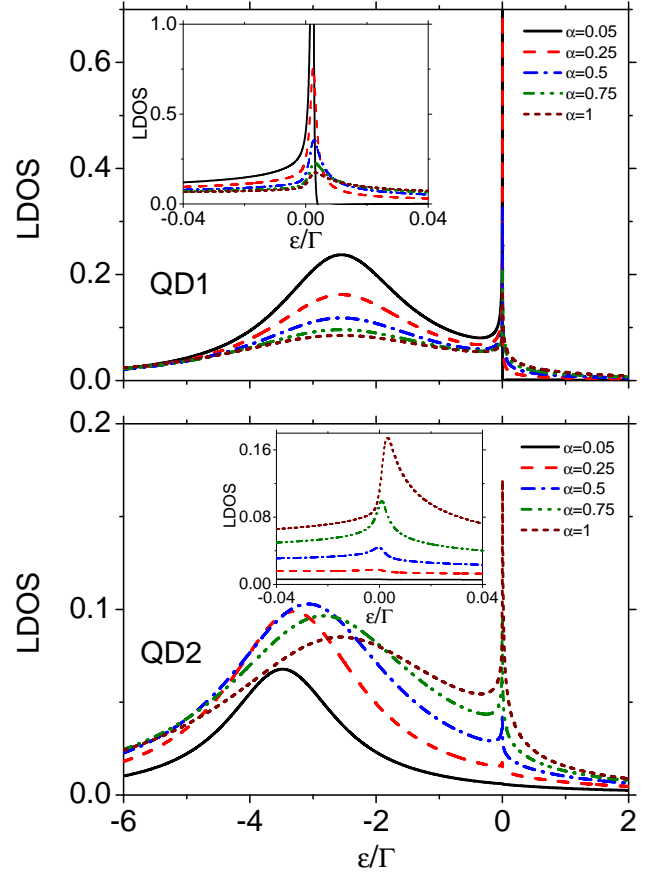


FIG. 4: Local density of states for the dots QD1 and QD2, calculated as a function of energy for indicated values of the parameter α . The other parameters are $\epsilon_0 = -3.5\Gamma$, $U = 50\Gamma$ and $t = 0$.

A. Numerical results for $t = 0$

Let us start with the case when the dots are capacitively coupled only, $t = 0$. The LDOS for both dots is plotted in Fig.4. The spectrum of each dot reveals two resonances corresponding to the dot level and its Coulomb counterpart (the latter not shown). Apart from this, a narrow peak emerges in the spectrum of each dot at the Fermi level of the leads. The intensity and width of this peak strongly depends on temperature, revealing all characteristic features typical of the Kondo resonance.

The resonance in LDOS originates from the many body processes which occur in the low temperature regime. Since the conditions $\epsilon_0 < \mu_{\beta i}$ and $\mu_{\beta i} < \epsilon_0 + U$ are obeyed for the parameters assumed (Coulomb blockade regime), only a single electron can occupy the DQD system and sequential tunnelling processes are blocked. However, higher-order tunnelling events are still allowed. Let us assume that an electron initially occupies the dot QD1, and the system is in the Coulomb blockade regime. Due to the uncertainty principle, the electron from the dot QD1 can tunnel onto the Fermi level of one of the leads

attached to QD1, while an electron from the Fermi level of one of the leads attached to QD2 can tunnel to the dot QD2 in the time $\hbar/|\epsilon_0|$. Interference of many such events gives rise to the narrow peaks in LDOS at the Fermi level.

For the fully symmetric model ($\alpha = 1$), LDOS for the dot QD1 is the same as that for QD2. The situation is different for $\alpha \neq 1$. As α decreases, the intensity of the Kondo peak in LDOS of the dot QD2 also decreases and disappears when α tends to zero. The opposite situation occurs in the LDOS of the dot QD1, where the Kondo peak becomes more and more pronounced with decreasing α . This behavior is due to the fact that the intensity of the Kondo peak in LDOS of the dot QD1 is mainly determined by the coupling strength between QD2 and the leads, while the Kondo peak for the dot QD2 is predominantly determined by coupling of the dot QD1 to the leads. Accordingly, the Kondo peak in LDOS of the dot QD1 (QD2) increases (decreases) with decreasing α , while the Kondo peaks of both dots are equal for $\alpha = 1$. This can be understood taking into account the maximal value of the conductance per each channel (each dot), which is equal to $G_i^{max} = e^2/h$. Estimating $G_i^{max} \sim \Gamma_{ii}(E_F)\rho_i(E_F)$ at the Fermi level, one obtains $\rho_1(E_F)/\rho_2(E_F) = 1/\alpha$, which explains the above behavior of the LDOS for QD1 and QD2. This behavior of the Kondo peaks in LDOS of both dots is similar to that in the case of spin Kondo effect, where each spin channel is coupled differently to the leads (when the leads are ferromagnetic).

For $\alpha \ll 1$, the Kondo peak for the dot QD1 becomes strongly asymmetric and the LDOS is totally suppressed for energies above the Fermi level, where the spectral function is equal to zero. This situation is similar to that reported in Ref.[19]. Apart from this, position of the Kondo peak for QD2 slightly moves away from the Fermi level with increasing α (towards positive energies), and becomes asymmetric for all values of α .

It is also worth to note that position of the broad maximum (associated with the dot's level) in LDOS of QD1 (the dot whose coupling to the leads changes with α) is almost unchanged with tuning α , whereas position of the broad maximum in the LDOS of the dot QD2 (coupled to the leads with constant strength) varies with the parameter α . This becomes clear when considering the formulas for renormalized dots' energy levels, Eq.(5). Apart from this, the intensity of the broad peak for the dot QD1 decreases monotonically with increasing α , whereas the intensity of the broad peak in the LDOS of the dot QD2 depends on α in a more complex way. When $\alpha \rightarrow 0$, the broad peak in the LDOS of the dot QD1 is then most pronounced, whereas its Coulomb counterpart (not shown) is totally localized at $\epsilon_0 + U$.

As mentioned before, the resonances in LDOS lead to zero bias anomaly in the differential conductance of the DQD system. Here, nonlinear conductance is defined in

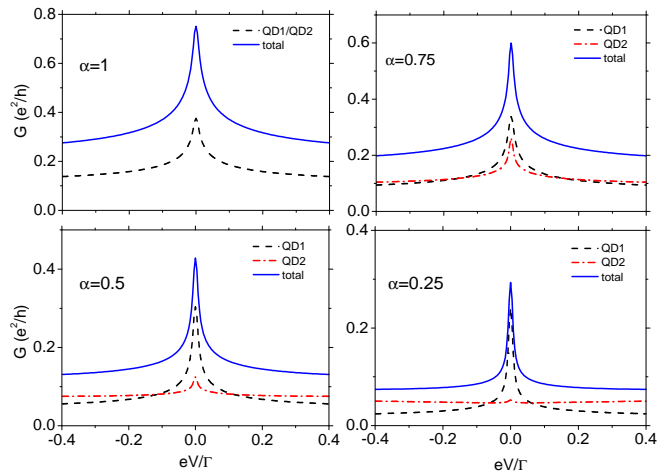


FIG. 5: Differential conductance for the dots QD1 and QD2, and the total differential conductance calculated for indicated values of α . The other parameters as in Fig.4.

the following way:

$$G = \frac{dJ}{dV}, \quad (23)$$

where J is current given by Meir and Wingreen formula²⁵. This quantity is very important from practical point of view as it is usually measured in QDs' experiments (to obtain basic transport properties of these systems)¹. In Fig.(5) we show the differential conductance of both dots as a function of the bias voltage. For a fully symmetric system, the differential conductance of both dots is the same, but the situation changes when α becomes smaller than 1, $\alpha < 1$. Interestingly, the conductance of the dot weakly coupled to the leads (in our case the dot QD1) is larger than the conductance of the dot strongly coupled to the leads. For a sufficiently small value of α , the differential conductance of the dot QD2 appears as a broad background, whereas the differential conductance of the dot weakly coupled to the leads is then very narrow. This behavior follows the features of LDOS of the dots QD1 and QD2 discussed above (Fig.4). Apart from this, we note that the total differential conductance diminishes as α decreases, and its line width also shrinks. This behavior indicates on the suppression of the effective Kondo temperature as α decreases. Such a behavior stems from the fact that the rate of tunneling events leading to the Kondo resonance decreases since the dot QD1 becomes detached from the leads as α decreases. This is also in agreement with our predictions on the α dependence of the Kondo temperature, derived in Sections III and IV (see also Fig.2). Finally, when one of the dot is totally disconnected from the leads ($\alpha = 0$), the Kondo temperature vanishes, and no Kondo effect appears.

When $\epsilon_1 \neq \epsilon_2$ (eg. when the level splitting due to renormalization is not compensated by external gate voltages), the Kondo peak in differential conductance becomes split

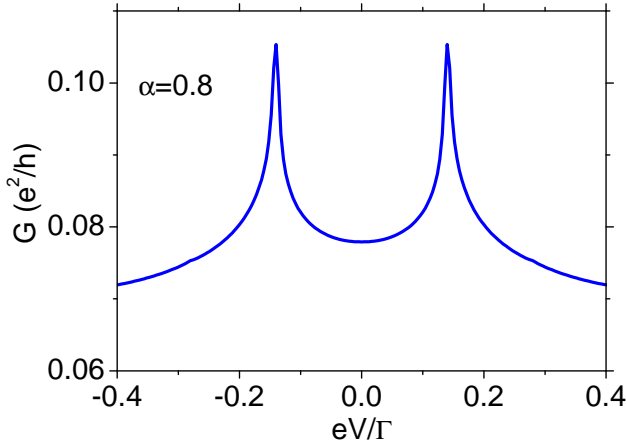


FIG. 6: Differential conductance calculated for indicated value of α in the case when the level slitting due to renormalization is not compensated by external gate voltages. The positions of the dots' levels have been estimated self-consistently using Eq.(5). The other parameters as in Fig.4.

and the two components are shifted from the Fermi level and have rather low intensity, as shown in Fig.6. This suppression of the Kondo anomaly resembles similar behavior in the case of the spin Kondo effect.

The presence of Kondo peaks also depends on the coupling strength of the dots to the leads. Above we assumed relatively strong coupling for both dots, with some asymmetry of this coupling described by the parameter α . We have also examined the case when both dots are weakly coupled to the leads. There is no Kondo effect in such a case, which is consistent with the recent experimental observations¹⁵.

B. Numerical results for the case $t \neq 0$

Now, we consider the situation when direct hopping between the dots is allowed. Figures 7 and 8 show LDOS for the dots QD1 and QD2. When both dots are equally coupled to the leads ($\alpha = 1$), a double peak structure emerges in the LDOS of the dots QD1 and QD2, and the LDOS is the same for both dots. The two peaks are centered at $\varepsilon = \pm 2t$. This comes from the fact that when $t \neq 0$, the dots' states hybridize into two molecular-like states with eigenenergies $\varepsilon_{\pm} = \varepsilon_0 \pm t$. These new states are then involved in the Kondo phenomenon. If initially an electron occupies the level ε_- , then it can tunnel into the Fermi level of a given lead and simultaneously another electron having energy $+2t$ tunnels onto the level ε_+ . Coherent superposition of many such events results in the Kondo peak at the energy $\varepsilon = 2t$. In the same way one may explain the presence of the Kondo peak at the energy $\varepsilon = -2t$.

However, the situation changes for $\alpha \neq 1$. Apart from the two peaks located at $\pm 2t$, one finds an additional

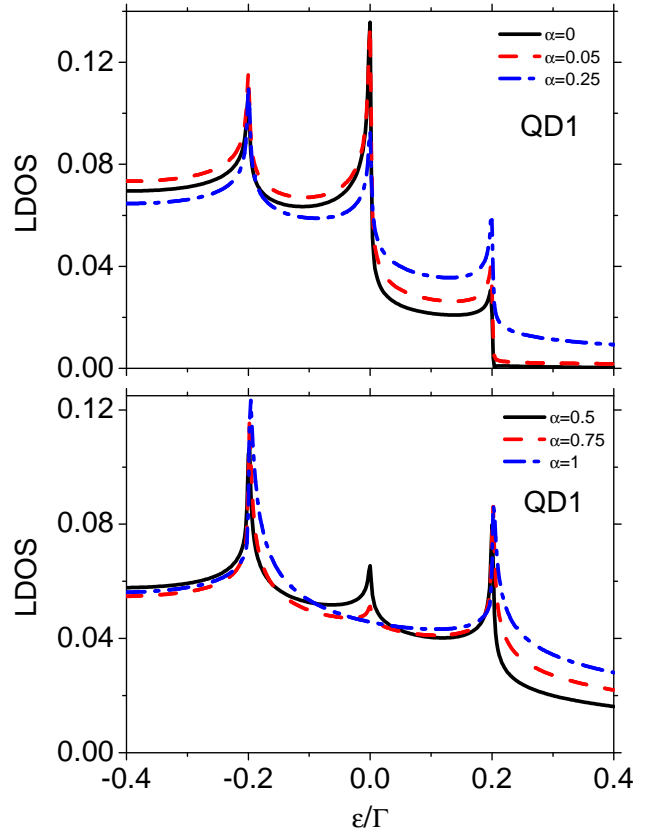


FIG. 7: Local density of states for the dot QD1, calculated for indicated values of α and for $t = -0.1\Gamma$. The other parameters as in Fig.4.

peak in the LDOS of the dot QD1, which is located at the Fermi level. However, instead of the peak, a dip in the LDOS of the dot QD2 appears at the Fermi level. Possible explanation of this behavior relies on the transitions/tunneling events which do not induce electron exchange between the molecular states ε_+ and ε_- , but rather between original bare dot levels. The appearance of the dip (at the Fermi level) can be explained using the arguments from Section V A. One can notice that for $\alpha = 1$ (symmetric couplings) there is no peak (or dip) in the LDOS at the Fermi level and LDOS for QD1 and QD2 are equal. For asymmetric couplings, i.e., $\alpha \neq 1$, the amplitude of the LDOS at the Fermi level for the dot weakly coupled to the leads exceeds that for the dot strongly coupled to the leads. As a result, the amplitude of the LDOS at the Fermi level for the dot strongly coupled to the leads decreases (as α decreases) and the dip structure occurs.

Differential conductance for several values of the asymmetry parameter α is shown in Fig.9. When the dots are connected in the T-shape geometry, $\alpha = 0$, one finds two maxima centered at $eV = \pm 2t$, and one dip at $eV = 0$. Suppression of the conductance at $eV = 0$ is a result of destructive quantum interference³¹. When the coupling to the dot QD1 is turned on, then the dip structure dis-

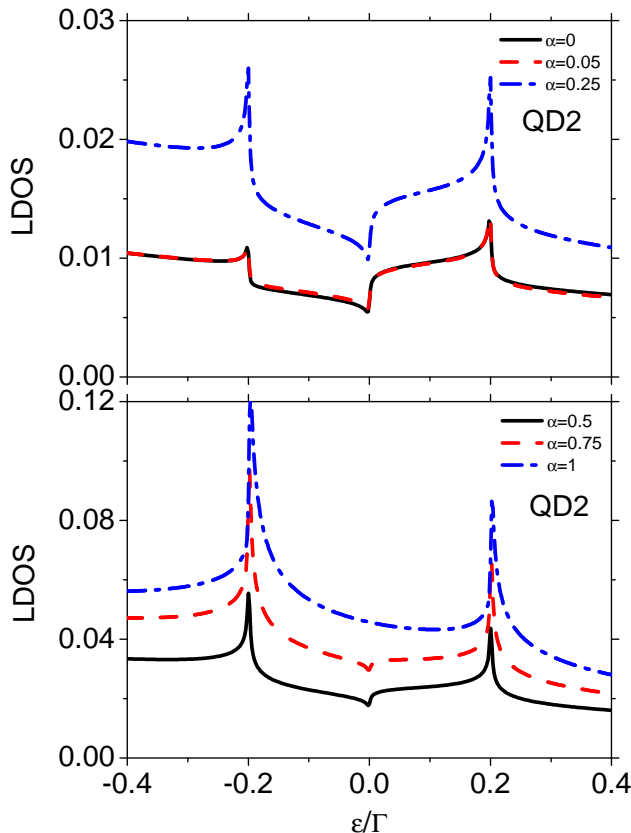


FIG. 8: Local density of states for the dot QD2, calculated for indicated values of α and for $t = -0.1\Gamma$. The other parameters as in Fig.4.

appears in the differential conductance. Instead of dip, one finds the third peak centered at $eV = 0$. For a fully symmetric system, $\alpha = 1$, this peak vanishes and only the satellite maxima are present. It is also worth to note that the conductance increases with increasing α .

VI. SUMMARY AND CONCLUSIONS

We have considered the orbital Kondo effect in a spinless system of two single-level quantum dots connected to electron reservoirs. Various techniques have been used to describe basic features of the Kondo physics. First, we used the scaling technique to evaluate the level renormalization and the corresponding Kondo temperature. Then, we used the slave boson technique to calculate local density of states and linear conductance. To find non-linear conductance we used the nonequilibrium Green function method.

The numerical results show that transport characteristics reveal typical Kondo phenomenon, similar to that observed in a single quantum dot with spin degenerate discrete level, coupled to external ferromagnetic leads. In the case considered, the splitting due to level renormalization could be compensated by external gate volt-

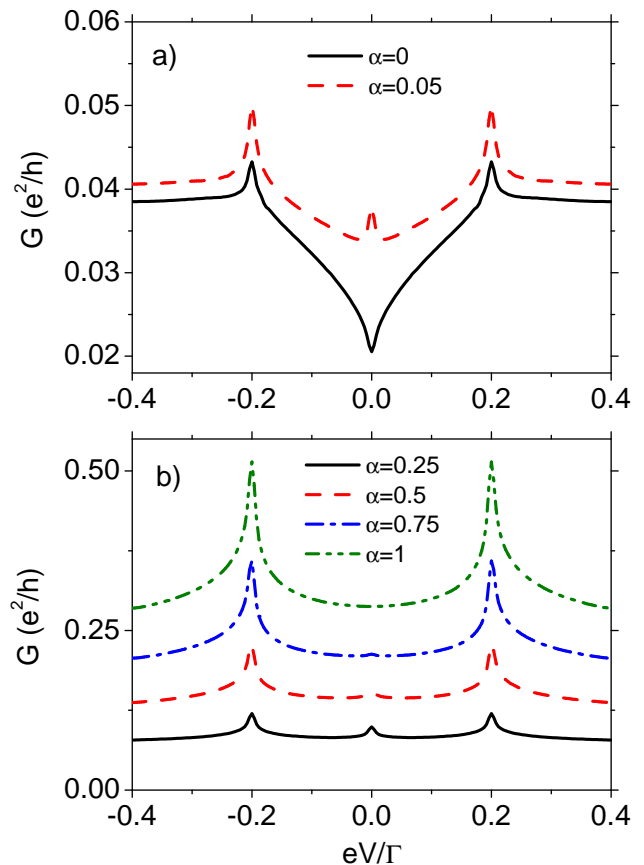


FIG. 9: Differential conductance for the dots QD1 and QD2, and total differential conductance calculated for indicated values of α and for $t = -0.1\Gamma$. The other parameters as in Fig.4.

ages, so one could reach the full Kondo anomaly. Such a compensation, however, is not possible when the direct tunneling between the dots is strong.

Acknowledgments

The author is extremely grateful to Prof. J. Barnaś for fruitful discussions and would like to thank him for giving helpful advices during preparation of the manuscript. This work, as part of the European Science Foundation EUROCORES Programme SPINTRA, was supported by funds from the Ministry of Science and Higher Education as a research project in years 2006-2009 and the EC Sixth Framework Programme, under Contract N. ERAS-CT-2003-980409. The author also acknowledges support by funds from Ministry of Science and Higher Education as a research project N N202 169536 in years 2009-2011.

Appendix: Green's functions

Here we show explicit form of the derived dots' Green functions G_{ij} for $i, j = 1, 2$;

$$G_{ii} = \frac{1}{M} \left\{ \left[1 + \frac{U}{W} (n_{\bar{i}} A_{\bar{i}} - n_{i\bar{i}} \tilde{t}) \right] \Omega_{\bar{i}\bar{i}} + \frac{U}{W} (n_{\bar{i}} \tilde{t} - n_{i\bar{i}} A_i) \Omega_{i\bar{i}} \right\}, \quad (\text{A.1})$$

$$G_{i\bar{i}} = \frac{1}{M} \left\{ \frac{U}{W} (n_i \tilde{t} - n_{i\bar{i}} A_{\bar{i}}) \Omega_{\bar{i}\bar{i}} + \left[1 + \frac{U}{W} (n_i A_i - n_{i\bar{i}} \tilde{t}) \right] \Omega_{i\bar{i}} \right\}, \quad (\text{A.2})$$

where

$$M = \Omega_{11} \Omega_{22} - \Omega_{12} \Omega_{21}$$

$$\Omega_{ii} = \epsilon - \epsilon_i - \Sigma_{ii}^{(0)} + \frac{U}{W} (\alpha_i A_{\bar{i}} + \gamma_i \tilde{t})$$

$$\Omega_{i\bar{i}} = t - \frac{U}{W} (\gamma_i A_{\bar{i}} + \alpha_{\bar{i}} \tilde{t}),$$

$$W = A_1 A_2 - \tilde{t}^2$$

$$A_1 = \epsilon - \epsilon_1 - U - \Sigma_{11}^{(0)} - \Sigma_{11}^c - \Sigma_{22}^e - \Sigma_{22}^d,$$

$$A_2 = \epsilon - \epsilon_2 - U - \Sigma_{22}^{(0)} - \Sigma_{22}^c - \Sigma_{11}^f - \Sigma_{11}^d,$$

$$\tilde{t} = t + \Sigma_{22}^a + \Sigma_{11}^b,$$

$$\alpha_1 = \Sigma_{22}^{dI} + \Sigma_{11}^{cI} + \Sigma_{22}^{eI},$$

$$\alpha_2 = \Sigma_{11}^{dI} + \Sigma_{11}^{fI} + \Sigma_{22}^{cI},$$

$$\gamma_1 = \Sigma_{22}^{aI} + \Sigma_{11}^{bI},$$

$$\gamma_2 = \Sigma_{22}^{aI} + \Sigma_{11}^{bI}.$$

The self-energies are defined in the following way

$$\Sigma_{ii}^{a(n)} = \sum_{\mathbf{k}\alpha} |V_{i\mathbf{k}}^\alpha|^2 \frac{t}{\Lambda} (\epsilon - \epsilon_{\mathbf{k}\alpha} + \Delta\epsilon) F_\alpha^{(n)}(\epsilon_{\mathbf{k}\alpha})$$

$$\Sigma_{ii}^{b(n)} = \sum_{\mathbf{k}\alpha} |V_{i\mathbf{k}}^\alpha|^2 \frac{t}{\Lambda} (\epsilon - \epsilon_{\mathbf{k}\alpha} - \Delta\epsilon) F_\alpha^{(n)}(\epsilon_{\mathbf{k}\alpha})$$

$$\Sigma_{ii}^{c(n)} = \sum_{\mathbf{k}\alpha} |V_{i\mathbf{k}}^\alpha|^2 \frac{2t^2}{\Lambda} F_\alpha^{(n)}(\epsilon_{\mathbf{k}\alpha})$$

$$\Sigma_{ii}^{d(n)} = \sum_{\mathbf{k}\alpha} \frac{|V_{i\mathbf{k}}^\alpha|^2}{\epsilon + \epsilon_{\mathbf{k}\alpha} - \epsilon_1 - \epsilon_2 - U} F_\alpha^{(n)}(\epsilon_{\mathbf{k}\alpha})$$

$$\Sigma_{ii}^{e(n)} = \sum_{\mathbf{k}\alpha} |V_{i\mathbf{k}}^\alpha|^2 \frac{t(\epsilon - \epsilon_{\mathbf{k}\alpha})(\epsilon - \epsilon_{\mathbf{k}\alpha} + \Delta\epsilon) - 2t^2}{\Lambda} F_\alpha^{(n)}(\epsilon_{\mathbf{k}\alpha})$$

$$\Sigma_{ii}^{f(n)} = \sum_{\mathbf{k}\alpha} |V_{i\mathbf{k}}^\alpha|^2 \frac{t(\epsilon - \epsilon_{\mathbf{k}\alpha})(\epsilon - \epsilon_{\mathbf{k}\alpha} - \Delta\epsilon) - 2t^2}{\Lambda} F_\alpha^{(n)}(\epsilon_{\mathbf{k}\alpha})$$

$$\Sigma_{ii}^{d(I)} = \sum_{\mathbf{k}\alpha} \frac{|V_{i\mathbf{k}}^\alpha|^2}{\epsilon - \epsilon_{\mathbf{k}\alpha}} f_\alpha(\epsilon_{\mathbf{k}\alpha})$$

with $\Lambda = (\epsilon - \epsilon_{\mathbf{k}\alpha})[(\epsilon - \epsilon_{\mathbf{k}\alpha} + \Delta\epsilon)(\epsilon - \epsilon_{\mathbf{k}\alpha} - \Delta\epsilon) - 4t^2]$, $\Delta\epsilon = \epsilon_1 - \epsilon_2$, $F_\alpha^{(n)}(\epsilon_{\mathbf{k}\alpha}) = f_\alpha(\epsilon_{\mathbf{k}\alpha})$ for $n = I$ and $F_\alpha^{(n)}(\epsilon_{\mathbf{k}\alpha}) = 1$

for $n = 0$. The self energy $\Sigma_{ij}^{(0)}$ is the self energy of the noninteracting system, i.e., $U = 0$ in the Hamiltonian (1).

Assuming that $\epsilon_1 = \epsilon_2 = \epsilon_0$ the self-energies including Fermi distribution function can be calculated analytically and expressed by means of digamma function.

Although, presented here EOM approach gives qualitatively good (physical) results around T_K , it breaks down (both qualitatively and quantitatively) at lower temperatures (especially at $T \ll T_K$). We must point out that the drawbacks in EOM method are due to the logarithmic divergence of the digamma function. Detailed analysis can be found in Ref.[33–36]. Here, we only list them briefly. Specifically, the divergence of the digamma function leads to wrong behavior of the linear conductance (density of states at the Fermi level)³⁵. Slave-boson calculations (which are exact at $T=0K$) show that the conductance saturates as the dot's level is decreased (see

Fig.3). This is no longer true for EOM approaches, where below certain dot's level position the conductance starts to decrease³⁵. The EOM methods, with different decoupling schemes^{4,33,36}, also do not conserve completeness relation as well as not satisfy Friedel sum rule³⁷. However, the decoupling schemes considered in our work somehow give surprisingly good dependence of the dot's occupation numbers as a function of the impurity level position (similar to those obtained by numerical renormalization group method³⁵). Taking all above into account one should remember that presented here EOM method leads to incorrect predictions at low temperatures and is limited to $T \gtrsim T_K$ as we stated in Section V. However, the EOM methods have an advantage on the other techniques used to investigate Kondo problem. Specifically, it enables to explore the non-equilibrium phenomena present in QDs systems biased by a finite voltage difference attached to the external leads.

* Electronic address: ptrocha@amu.edu.pl

- ¹ S. M. Cronenwett et al., Science **281**, 540 (1998); S. Sasaki, S. De Franceschi, J. M. Elzerman, W. G. van der Wiel, M. Eto, S. Tarucha, and L. P. Kouwenhoven, Nature (London) **405**, 764 (2000).
- ² J. Gores, D. Goldhaber-Gordon, S. Heemeyer, M. A. Kastner, H. Shtrikman, D. Mahalu, and U. Meirav, Phys. Rev. B **62**, 2188 (2000).
- ³ L. I. Glazman and M. E. Raikh, JETP Lett. **47**, 452 (1988); T. K. Ng and P. A. Lee, Phys. Rev. Lett. **61**, 1768 (1988).
- ⁴ Y. Meir, N. S. Wingreen, and P. A. Lee, Phys. Lett. **66**, 3048 (1991); Phys. Lett. **70**, 2601 (1993).
- ⁵ K. Kang and B. I. Min, Phys. Rev. B **52**, 10689 (1995).
- ⁶ P. Nordlander, M. Pustilnik, Y. Meir, N. S. Wingreen, and D. C. Langreth, Phys. Lett. **83**, 808 (1999).
- ⁷ R. Aguado and D. C. Langreth, Phys. Rev. Lett. **85**, 1946 (2000); R. López, R. Aguado, and G. Platero, Phys. Rev. Lett. **89**, 136802 (2002); R. Aguado and D. C. Langreth, Phys. Rev. B **67**, 245307 (2003).
- ⁸ T. Aono and M. Eto, Phys. Rev. B **63**, 125327 (2001).
- ⁹ R. Świrkowicz, J. Barnaś, and M. Wilczyński, Phys. Rev. B **68**, 195318 (2003); R. Świrkowicz, M. Wilczyński, M. Wawrzyniak, and J. Barnaś, Phys. Rev. B **73**, 193312 (2006); R. Świrkowicz, M. Wilczyński, and J. Barnaś, J. Phys.: Condens. Matter **18**, 2291 (2006).
- ¹⁰ T. Kuzmenko, K. Kikoin, Y. Avishai, Phys. Rev. B **69**, 195109 (2004); Phys. Rev. Lett. **96**, 046601 (2006).
- ¹¹ J. S. Lim, M.-S. Choi, R. López, and R. Aguado, Phys. Rev. B **74**, 205119 (2006).
- ¹² G. Grüner and A. Zawadowski, Rep. Prog. Phys. **37**, 1497 (1974); G. Zarád and A. Zawadowski, Phys. Rev. Lett. **72**, 542 (1994).
- ¹³ D. Boese, W. Hofstetter, and H. Schoeller, Phys. Rev. B **64**, 125309 (2001).
- ¹⁴ P. G. Silvestrov and Y. Imry, Phys. Rev. B **75**, 115335 (2007).
- ¹⁵ A. Hübner, K. Held, J. Weis, and K. v. Klitzing, Phys. Rev. Lett. **101**, 186804 (2008).
- ¹⁶ U. Wilhelm, J. Schmid, J. Weis, K.v. Klitzing, Physica

- (Amsterdam) **14E**, 385 (2002).
- ¹⁷ Q.-F. Sun and H. Guo, Phys. Rev. B **66**, 155308 (2002).
- ¹⁸ D. Sztienkiel and R. Świrkowicz, J. Phys.: Condens. Matter **19**, 256205 (2007).
- ¹⁹ D. Sztienkiel and R. Świrkowicz, J. Phys.: Condens. Matter **19**, 386224 (2007).
- ²⁰ A. W. Holleitner, A. Chudnovskiy, D. Pfannkuche, K. Eberl, and R. H. Blick, Phys. Rev. B **70**, 075204 (2004).
- ²¹ S. Lipiński and D. Krychowski, Phys. Status Solidi b **243**, 206 (2005).
- ²² T. Pohjola, H. Schoeller, and G. Schön, Europhys. Lett., **54**, 241 (2001).
- ²³ J. Wen, J. Peng, B. Wang, and D. Y. Xing, Phys. Rev. B **75**, 155327 (2007).
- ²⁴ T. Kubo, Y. Tokura, and S. Tarucha, Phys. Rev. B **77**, 041305(R) (2008).
- ²⁵ Y. Meir, N. S. Wingreen, Phys. Rev. Lett. **68**, 2512 (1992).
- ²⁶ A. C. Hewson, The Kondo Problem to Heavy Fermions (Cambridge University Press, Cambridge, U.K., 1993).
- ²⁷ J. Martinek, Y. Utsumi, H. Imamura, J. Barnaś, S. Maekawa, J. König, and G. Schön, Phys. Lett. **91**, 127203 (2003); D. Matsubayashi and M. Eto, Phys. Rev. B **75**, 165319 (2007).
- ²⁸ V. Kashcheyevs, A. Schiller, A. Aharony, and O. Entin-Wohlman, Phys. Rev. B **75**, 115313 (2007).
- ²⁹ P. Coleman, Phys. Rev. B **29**, 3036 (1984).
- ³⁰ T. K. Ng, Phys. Rev. Lett., **3635** (1993).
- ³¹ P. Trocha, J. Barnaś, Phys. Rev. B **76**, 165432 (2007).
- ³² P. Trocha and J. Barnaś, J. Nanosci. Nanotechnol. **10**, 2489 (2010).
- ³³ C. Lacroix, J. Appl. Phys **53**, 2131 (1982).
- ³⁴ T. A. Costi, J. Phys. C: Solid State Phys. **19**, 5665 (1986).
- ³⁵ T. Lobo, M.S. Figueira, R. Franco, J. Silva-Valencia, and M.E. Foglio, Physica B **398**, 446 (2007).
- ³⁶ H.-G. Luo, J.-J. Ying, and S.-J. Wang, Phys. Rev. B **59**, 9710 (1999).
- ³⁷ T. Lobo, M. S. Figueira, and M. E. Foglio, Nanotechnology **17**, 6016 (2006); *ibid* **21**, 274007 (2010).